Effector membrane translocation biosensors reveal G protein and βarrestin coupling profiles of 100 therapeutically relevant GPCRs

Charlotte Avet[1†], Arturo Mancini[2†], Billy Breton[2‡§], Christian Le Gouill[1‡], Alexander S. Hauser[3‡], Claire Normand[2], Hiroyuki Kobayashi[1], Florence Gross[2], Mireille Hogue[1], Viktoriya Lukasheva[1], Stéphane St-Onge[1], Marilyn Carrier[1], Madeleine Héroux[1], Sandra Morissette[2], Eric Fauman[4], Jean-Philippe Fortin[5], Stephan Schann[6], Xavier Leroy[6*], David E. Gloriam[3*], and Michel Bouvier[1*].

[1]*Institute for Research in Immunology and Cancer (IRIC), and Department of Biochemistry and Molecular Medicine, Université de Montréal; Montréal, Québec, H3T 1J4, Canada.*
[2]*Domain Therapeutics North America; Montréal, Québec, H4S 1Z9, Canada.*
[3]*Department of Drug Design and Pharmacology; University of Copenhagen; 2100 Copenhagen, Denmark.*
[4]*Internal Medicine Research Unit; Pfizer Worldwide Research, Development and Medical; Cambridge, MA 02139, USA.*
[5]*Pfizer Global R&D; Cambridge, MA 02139, USA.*
[6]*Domain Therapeutics; 67400 Illkirch-Strasbourg, France.*
[†]*These authors contributed equally.*
[‡]*These authors contributed equally.*
[§]*Current address: Institute for Research in Immunology and Cancer (IRIC), Université de Montréal; Montréal, Québec, H3T 1J4, Canada.*

*** Corresponding authors**:

Michel Bouvier ; IRIC, Université de Montréal : michel.bouvier@umontreal.ca,

David E. Gloriam; University of Copenhagen: david.gloriam@sund.ku.dk,

Xavier Leroy; Domain Therapeutics: xleroy@domaintherapeutics.com

Summary

The recognition that individual GPCR can engage multiple signaling pathways has raised the possibility of developing drugs selectively targeting therapeutically relevant ones. This requires tools to determine which G proteins and βarrestins are engaged by a given receptor. Here, we present a set of BRET sensors monitoring the activation of the 12 G protein subtypes based on the translocation of their effectors to the plasma membrane (EMTA). Unlike most of the existing detection systems, EMTA does not require modification of receptors or G proteins (except for G_s). EMTA was found to be suitable for the detection of constitutive activity, inverse agonism, biased signaling and polypharmacology. Profiling of 100 therapeutically relevant human GPCRs resulted in 1,500 pathway-specific concentration-response curves and revealed a great diversity of coupling profiles ranging from exquisite selectivity to broad promiscuity. Overall, this work describes unique resources for studying the complexities underlying GPCR signaling and pharmacology.

Introduction

G protein-coupled receptors (GPCRs) play crucial roles in the regulation of a wide variety of physiological processes and represent one-third of clinically prescribed drugs (Hauser, Attwood, Rask-Andersen, Schioth, & Gloriam, 2017). Classically, GPCR-mediated signal transduction was believed to rely on linear signaling pathways whereby a given GPCR selectively engages a single G protein family, defined by the nature of its Gα subunit (Oldham & Hamm, 2008). Gα proteins are divided into four major families (G_s, $G_{i/o}$, $G_{q/11}$, and $G_{12/13}$) encoded by 16 human genes. Once activated, these proteins each engage different downstream effectors yielding different biological outcomes. It has now become clear that many GPCRs can engage more than one G protein family and that ligands can selectively promote the engagement of different subsets of these pathways (Namkung et al., 2018; Quoyer et al., 2013). These observations extended the concept of ligand-biased signaling, which was first established for ligand-directed selectivity between βarrestin and G protein (Azzi et al., 2003; Wei et al., 2003), to functional selectivity between G proteins. Ligand-directed functional selectivity represents a promising avenue for GPCRs drug discovery since it offers the opportunity of activating pathways important for therapeutic efficacy while minimizing engagement of pathways responsible for undesirable side effects (Galandrin, Oligny-Longpre, & Bouvier, 2007; Kenakin, 2019).

To fully explore the potential of functional selectivity, it is essential to have an exhaustive description of the signaling partners that can be engaged by a given receptor, providing receptor- and ligand-specific signaling signatures. Currently, few assays allow for an exhaustive pathway-specific analysis of GPCR signaling; these include BRET-based G protein activation sensors platforms (Gales et al., 2005; Masuho et al., 2015; Maziarz et al., 2020; Mende et al., 2018; Olsen et al., 2020) and the TGF-α shedding assay (Inoue et al., 2019). However, several of these platforms require modification of G protein subunits that may create functional distortions. Moreover, these assays may detect non-productive conformational rearrangements of the G protein heterotrimer as was recently reported for G_{12} (Okashah et al., 2020).

Here, we describe unique sensors that do not require modification of receptors or G proteins for interrogating the signaling profiles of GPCRs. The platform includes 15 pathway-selective enhanced bystander bioluminescence resonance energy transfer (ebBRET) biosensors monitoring the translocation of downstream effectors to the plasma membrane for $G_{i/o}$, $G_{q/11}$ and $G_{12/13}$, the dissociation of the Gα subunit from the plasma membrane for G_s and the recruitment of βarrestin to the plasma membrane. Overall, the new ebBRET-based **E**ffector **M**embrane **T**ranslocation **A**ssays, named EMTA, provide a readily accessible large scale and comprehensive platform to study constitutive and ligand-directed GPCR signaling. The signaling signatures of 100 GPCRs using the EMTA platform also provides a rich source of information to explore the principles underlying receptor/G protein/βarrestin coupling selectivity relationships.

Results

ebBRET-based G protein effector membrane translocation assay (EMTA) allows detection of each Gα protein subunit activation

To detect the activation of Gα subtypes, we created an EMTA biosensor platform based on ebBRET (Namkung et al., 2016) (**Figure 1A**). The biosensors at the heart of EMTA consist of sub-domains of the G protein-effector proteins p63-RhoGEF, Rap1GAP and PDZ-RhoGEF that selectively interact with activated $G_{q/11}$, $G_{i/o}$ or $G_{12/13}$, respectively. These domains were fused at their C-terminus to *Renilla* luciferase (RlucII) and co-expressed with different unmodified receptor and Gα protein subtypes. Upon GPCR activation, the energy donor-fused effectors translocate to the plasma membrane to bind activated Gα proteins, bringing RlucII in close proximity to the energy acceptor, *Renilla* green fluorescent protein, targeted to the plasma membrane through a CAAX motif (rGFP-CAAX), thus leading to an increase in ebBRET. The same plasma membrane translocation principle is used to measure βarrestin recruitment (Namkung et al., 2016) (**Figure 1B,** top). Because no selective soluble downstream effector of G_s exists, the assay was modified taking advantage of $G\alpha_s$ dissociation from the plasma membrane following its activation (Wedegaertner, Bourne, & von Zastrow, 1996). In this configuration, the RlucII is directly fused to $G\alpha_s$ (Carr et al., 2014). Its activation upon GPCR stimulation leads to its dissociation from the plasma membrane (Martin & Lambert, 2016), resulting in a reduction in ebBRET (**Figure 1B,** bottom).

The sensitivity and selectivity of the newly created G protein EMTA biosensors, were validated using prototypical GPCRs known to activate specific Gα subtypes. The responses were monitored upon heterologous expression of specific Gα subunits belonging to $G_{i/o}$, $G_{q/11}$ or $G_{12/13}$ families in the absence or presence of pharmacological inhibitors and using engineered cells lacking selected Gα subtypes. The dopamine D_2 receptor was used to validate the ability of the $G_{i/o}$ binding domain of Rap1GAP (Jordan, Carey, Stork, & Iyengar, 1999; Meng, Glick, Polakis, & Casey, 1999) to selectively detect $G_{i/o}$ activation. The dopamine-promoted increase in ebBRET between Rap1GAP-RlucII and rGFP-CAAX in the

presence of $G\alpha_{i/o}$ subunits was not affected by the $G_{q/11}$-selective inhibitor UBO-QIC (a.k.a., FR900359 (Schrage et al., 2015); **Figure 2A**, left), whereas the $G\alpha_{i/o}$ family inhibitor, pertussis toxin (PTX), completely blocked the response for all members of $G\alpha_{i/o}$ family except for $G\alpha_z$, known to be insensitive to PTX (Casey, Fong, Simon, & Gilman, 1990) (**Figure 2A**, right). The gonadotropin-releasing hormone receptor (GnRHR), used as a prototypical $G_{q/11}$-coupled receptor, promoted ebBRET between the RlucII-fused $G_{q/11}$ binding domain of p63-RhoGEF (p63-RhoGEF-RlucII) (Lutz et al., 2007; Rojas et al., 2007) and rGFP-CAAX. The ebBRET increase observed in the presence of different $G\alpha_{q/11}$ subunits was not affected by PTX (**Figure 2B**, right), whereas UBO-QIC completely blocked the response for all members of $G\alpha_{q/11}$ family except for $G\alpha_{15}$, known to be insensitive to UBO-QIC (Schrage et al., 2015) (**Figure 2B**, left). These two G protein specific EMTA were sensitive enough to detect responses elicited by endogenous G protein since deletion of $G_{i/o}$ ($\Delta G_{i/o}$) or $G_{q/11}$ ($\Delta G_{q/11}$) subtypes completely abolished the responses induced by D_2 or GnRHR activation (**Figure S1I**). The selectivity of the $G_{12/13}$ binding domain of PDZ-RhoGEF (Fukuhara, Chikumi, & Gutkind, 2001) was confirmed using the cannabinoid receptor type 1 (CB_1). The ebBRET between PDZ-RhoGEF-RlucII and rGFP-CAAX in the presence of $G\alpha_{12}$ or $G\alpha_{13}$ promoted by the cannabinoid agonist WIN-55,212-2 was not affected by UBO-QIC (**Figure 2C**, top left), nor PTX (**Figure 2C**, top right). Given the lack of selective $G_{12/13}$ pharmacological inhibitor, we used HEK293 cells genetically deleted for $G\alpha_{12}$ and $G\alpha_{13}$ proteins ($\Delta G_{12/13}$) to further confirm the response selectivity. As expected, PDZ-RhoGEF-RlucII/rGFP-CAAX ebBRET was observed only following reintroduction of either $G\alpha_{12}$ ($\Delta G_{12/13}$_+G_{12}) or $G\alpha_{13}$ ($\Delta G_{12/13}$_+G_{13}) (**Figure 2C**, bottom left). The $G_{12/13}$ coupling of CB1 was further confirmed by monitoring the recruitment of PKN to the plasma membrane (**Figure 2C**, bottom right) in agreement with previous reports (Inoue et al., 2019).

To further assess the selectivity of each EMTA biosensor, we took advantage of the fact that the endothelin-1 receptor (ET_A) can activate $G_{q/11}$, $G_{i/o}$ and $G_{12/13}$ family members. As shown in **Figure S2**, only over-expression of the Gα family members corresponding to their selective effectors (Rap1GAP for $G_{i/o}$, p63-RhoGEF for $G_{q/11}$ and PDZ-RhoGEF for

$G_{12/13}$) significantly increased the recruitment of the effector-RlucII to the plasma membrane. It should also be noted that in the heterologous expression configuration, competition with endogenous G proteins did not occur to a significant extent since the potencies of the responses to a given G protein subtype were not affected by genetic deletion of the different G protein family members (**Figure S1** and **Supplementary Table 1**). In addition to spectrometric assessment of coupling selectivity (above) and activation kinetics (**Figure S3**), EMTA allows to image the real-time recruitment of the G protein effectors to the plasma membrane (**Videos 1-3**) thus providing spatiotemporal resolution for the imaging detection of $G\alpha_{i/o}$, $G\alpha_{q/11,14,15}$ and $G\alpha_{12/13}$ activation.

For the $G\alpha_s$ translocation biosensor, the bile acid receptor (GPBA) was chosen for validation (Kawamata et al., 2003). As expected, lithocholic acid stimulation resulted in a concentration-dependent decrease in ebBRET between $G\alpha_s$-RlucII and rGFP-CAAX (**Figure 2D**, left). Cholera toxin (CTX), which directly activates $G\alpha_s$ (De Haan & Hirst, 2004), led to a decrease in ebBRET (**Figure 2D**, center), confirming that loss of $G\alpha_s$ plasma membrane localization results from its activation. The potency of lithocholic acid to promote G_s dissociation from the plasma membrane was well in line with its potency to increase cAMP production as assessed using a BRET²-based EPAC biosensor (Leduc et al., 2009) (**Figure 2D**, right). The G_s-plasma membrane dissociation ebBRET signal was not affected by UBO-QIC or PTX (**Figure 2D**, left), confirming the selectivity of the biosensor.

Signaling signatures of one hundred therapeutically relevant receptors reveals distinct G protein and βarrestin selectivity profiles

We used EMTA to assess the signaling signature of a panel of 100 therapeutically relevant human GPCRs. For each receptor, we quantified its ability to activate 15 pathways: $G\alpha_s$, $G\alpha_{i1}$, $G\alpha_{i2}$, $G\alpha_{oA}$, $G\alpha_{oB}$, $G\alpha_z$, $G\alpha_{12}$, $G\alpha_{13}$, $G\alpha_q$, $G\alpha_{11}$, $G\alpha_{14}$, $G\alpha_{15}$ and βarrestin 2 as well as βarrestin 1 and 2 in presence of GRK2 (**Supplementary File 1**). E_{max} and pEC_{50} values were determined (**Supplementary Table 2**) and, based on the pre-determined threshold criteria (Emax ≥ mean of vehicle-stimulated + 2*SD; see Methods), a 'yes or no' agonist-

dependent activation was assigned to each signaling pathway and summarized using radial graph representations (**Figure S4**). To assess whether endogenous receptors could contribute to the observed responses, assays were also carried out in cells not transfected with the studied receptor (**Figure S5**). When an agonist-promoted response was observed in non-transfected parental HEK293 cells, this response was not considered as a receptor-specific response (see Methods).

To compare the signaling profiles across all receptors and pathways and to overcome differences in receptor expression levels and individual biosensor dynamic window, we first normalized E_{max} and pEC_{50} values (between 0 and 1) across receptors as a function of a reference receptor yielding the largest response for a given pathway (**Figure 3A**, left). Then, these values were normalized between 0 and 1 for the same receptor across pathways, using the pathway with the largest response for this receptor as the reference (**Figure 3A**, right; see description in Methods). Such double normalization allows direct comparison of the coupling efficiency to different G proteins for a given receptor and across receptors for a given G protein. This coupling efficiency is summarized as heatmaps (**Figure 3B**) that reveals a high diversity of signaling profiles. The selectivity toward the different G protein families varies considerably among GPCRs (**Figure 4**). In our dataset which is the first using unmodified GPCRs and Gα proteins, 29% of the receptors coupled to only one family, whereas others displayed more promiscuity by coupling to 2, 3 or 4 families (36%, 25% and 10% respectively). Receptors coupling to a single G protein family favored the members of the $G_{i/o}$ family. Indeed, 27% of the receptors coupling to $G_{i/o}$ only engaged this subtype family in comparison to 0, 2.4 and 9.1% for receptors activating $G_{12/13}$, $G_{q/11}$ and G_s, respectively, thus displaying more promiscuous coupling. A detailed analysis of the selectivity profiles and comparison with existing data sets is presented in the accompanying paper (Hauser et al., 2021).

When examining the frequency of coupling for each Gα subunit family (**Figure 4C**), the $G_{i/o}$ family members were the most commonly activated, with 89% of the tested receptors

activating a $G_{i/o}$ family member. In contrast, only 33%, 49% and 45% of the receptors engaged G_{s}, $G_{12/13}$ or $G_{q/11}$ (excluding $G\alpha_{15}$) family members, respectively. Not surprisingly, and consistent with its reported promiscuous coupling, $G\alpha_{15}$ was found to be activated by 81% of the receptors. For some receptors, we also observed preferential engagement of distinct members within a subtype family (**Figure S4**). For instance, 33% of $G_{i/o}$-coupled receptors can engage only a subpopulation of the family (**Figure S6A**). For the $G_{q/11}$ family, only 44% engaged all family members with 45% engaging only $G\alpha_{15}$ and 11% engaging only 2 or 3 members of the family. A matrix expressing the % of receptors engaging a specific Gα subtype that also activated another subtype, is illustrated in **Figure S6B.** When considering the correlation within families, considerable variations within the $G_{i/o}$ family were observed. The correlation is the strongest between $G\alpha_{oB}$ and either $G\alpha_{oA}$ or $G\alpha_{z}$, and the weakest between $G\alpha_{i1}$ and $G\alpha_{z}$. A striking example of intra-family coupling selectivity is the serotonin 5-HT_{2B} that engages only $G\alpha_{oB}$ and $G\alpha_{z}$ and GPR56 that selectively engages $G\alpha_{oB}$. Similarly, when considering the ligand-promoted responses above our threshold criteria (see Methods), histamine H_2 and melanocortin MC3 receptors show preferred engagement to $G\alpha_{oB}$ and $G\alpha_{z}$, whereas the prostaglandin F (FP) and neuropeptide Y5 (Y_5) receptors preferentially activate $G\alpha_{oB}$, $G\alpha_{oA}$ and $G\alpha_{z}$.

When considering βarrestin recruitment, our analysis shows that 22% of receptors did not recruit βarrestin, even in the presence of overexpressed GRK2 (**Figure 4D**). Among the receptors able to recruit βarrestins, only a very small number selectively recruited βarrestin1 (1.3%) or βarrestin2 (6.4%), most of them recruiting both βarrestins in the presence of GRK2 (92.3%) (**Figure 4D**). Overexpression of GRK2 potentiated the recruitment of βarrestin2 for 68% of receptors highlighting the importance of GRK2 expression level in determining βarrestin engagement (**Supplementary File 1** and **Supplementary Table 2**).

Validation of newly identified $G_{12/13}$ and G_{15} coupling

In the companion paper (Hauser et al., 2021), we compared the signaling profiles that we observed using the EMTA sensors with that of the chimeric G protein-based assay developed by Inoue *et al.* (Inoue et al., 2019) and the IUPHAR/BPS Guide to Pharmacology database (GtP; https://www.guidetopharmacology.org/). This comparative analysis revealed a number of couplings that were not reported in either GtP database or Inoue *et al.* study (Inoue et al., 2019). EMTA identified 25 receptors that were not reported to couple to either G_{12} or G_{13} when using the same threshold on the three datasets (see companion paper (Hauser et al., 2021)). Similarly, 45 new receptor couplings to G_{15} were identified with EMTA. It could be argued that the ability to detect a greater number of couplings could be due to the exogenous expression of the G proteins themselves. However, such heterologous expression is used in most assays directly detecting G protein activation, including the chimeric G proteins-based assay reported in Inoue et al. (Inoue et al., 2019), suggesting that EMTA may be more sensitive to detect possible couplings. For $G_{12/13}$ and G_{15} specifically, the difference with the GtP dataset most likely results from the fact that in most cases $G_{12/13}$ or G_{15} activation were determined indirectly since until their recent description ($G_{12/13}$: (Quoyer et al., 2013; Schrage et al., 2015); G_{15}:(Inoue et al., 2019; Olsen et al., 2020)) no robust amenable assays existed to monitor the activation of these G proteins.

To validate the newly identified $G_{12/13}$ couplings, we used the orthogonal PKN-based BRET biosensor detecting RhoA activation downstream of either $G_{12/13}$ or $G_{q/11}$ (Namkung et al., 2018). Ligand stimulation of FP and cysteinyl leukotriene 2 ($CysLT_2$) receptors led to a RhoA activation that was insensitive to the $G_{q/11}$ inhibitor YM-254890 (**Figure S7A**), confirming that these receptors signal through $G\alpha_{12/13}$.

Newly identified G_{15} couplings were confirmed taking advantage of the lack of $G\alpha_{15}$ in HEK293 cells and assessing the impact of $G\alpha_{15}$ heterologous expression on receptor-mediated calcium responses (**Figure S7B**). For prostaglandin E2 (EP_2) and κ-opioid (κOR) receptors, which couple to G_{15} but no other $G_{q/11}$ members, expression of $G\alpha_{15}$

significantly increased the PGE2- and dynorphin A- promoted calcium responses. For α_{2A} adrenergic (α_{2A}AR) and vasopressin 2 (V_2) receptors that couple other $G_{q/11}$ family members, treatment with YM-254890 completely abolished the agonist-promoted calcium response in the absence of $G\alpha_{15}$. In contrast, the calcium response evoked by α_{2A}AR and V_2 agonists following $G\alpha_{15}$ expression was completely insensitive to YM-254890 (**Figure S7B**), confirming that these receptors can activate this YM-254890-insensitive G protein subtype (Takasaki et al., 2004).

EMTA platform detects constitutive receptor activity and biased signaling

We went on to assess the ability of the EMTA platform to detect receptor constitutive activity. Transfection of increasing amounts of adenosine A_1 receptor (A_1) led to a receptor-dependent increase in basal (ligand-independent) ebBRET of the $G\alpha_{i2}$-activation sensor (**Figure 5A**, left), reflecting A_1 constitutive activity. Whereas adenosine further increased $G\alpha_{i2}$-activation, the A_1 inverse agonist DPCPX (Lu et al., 2014) dose-dependently decreased the constitutive A_1-mediated activation of $G\alpha_{i2}$ (**Figure 5A**, right). EMTA also faithfully detected biased signaling as illustrated by the ability of the G_q, G_{i2}, G_{13} and βarrestin2 sensors to distinguish the unbiased type-1 angiotensin II receptor (AT_1) agonist angiotensin from previously reported (Namkung et al., 2018) βarrestin-biased AT_1 ligands (**Figure 5B**). The platform was also used to identify biased-signaling resulting from single nucleotide polymorphisms. As shown in **Figure 5C**, two naturally occurring variants of human GPR17 (isoform 2) localised in the TM3 E/DRY motif resulted in altered functional selectivity profiles. Whereas the Asp128Asn variant displayed WT-like activity on $G\alpha_{i2}$, it lost the ability to engage $G\alpha_q$ and βarrestin2. In contrast, variant Arg129His at the neighboring position resulted in an increased constitutive βarrestin2 recruitment and a loss of $G\alpha_{i2}$ and $G\alpha_q$ protein signaling.

Combining G_z and G_{15} biosensors for safety panels and systems pharmacology

The G protein coupling profiles obtained for the 100 GPCRs revealed that 95% of receptors activate either $G\alpha_z$ (73%) or $G\alpha_{15}$ (81%). Measuring activation of both pathways

simultaneously provides an almost universal sensor applicable to screening. Combining the two sensors (Rap1GAP-RlucII/p63-RhoGEF-RlucII/rGFP-CAAX) in the same cells allowed to detect ligand concentration-dependent activation of a safety panel of 24 GPCRs (Bowes et al., 2012) (**Figure S8**)**.** Indeed, the G_z/G_{15} sensor captured the activation of receptors largely or uniquely coupled to either $G\alpha_z$ (e.g., CB_2) or $G\alpha_{15}$ (e.g., A_{2A}), as well as receptors coupled (to varying degrees) to both pathways. The usefulness of the G_z/G_{15} combined sensor to detect off-target ligand activity is illustrated in **Figure 6A**. Most ligands tested were specific for their primary target(s). However, certain ligands displayed functional cross-reactivity with GPCRs other than their cognate targets. These included the activation of the CB_1 and CB_2 receptors by acetylcholine, α_{2A}AR by dopamine and serotonin, and of the D_2 by noradrenaline and serotonin. The direct activation of D_2 by noradrenaline and serotonin was confirmed by the ability of the D_2-selective antagonist eticlopride to block the dopamine, serotonin and noradrenaline responses detected using the combined G_z/G_{15} or the canonical sG_{i2}, G_{oB} and βarrestin2 (**Figure 6B**, top). Similarly, use of the selective α_{2A}AR antagonist WB4101 allowed to confirm that dopamine can directly activate $G\alpha_{i2}$, $G\alpha_{oB}$ and βarrestin2 through the α_{2A}AR (**Figure 6B**, bottom). Such pleiotropic activation of different monoaminergic receptors by catecholamines and serotonin has been previously observed.

In contrast with what was observed in the case of the monoaminergic ligand and receptors discussed above, the activation of cannabinoid CB_1 and CB_2 receptors by acetylcholine (detected by the $G_{z/15}$ and confirmed with the G_{oB} sensors; **Figure 6A**, **C**) resulted from a "trans"-effect, where the tested receptor is indirectly activated following activation of an endogenous receptor responding to the tested ligand. Indeed, the activation was completely inhibited by the CB inverse agonist AM-630 but also by the cholinergic antagonist atropine (**Figure 6C**, left). Yet the response evoked by the CB selective agonist WIN55,212 2 was not blocked by atropine (**Figure 6C**, center). $G\alpha_{oB}$ activation by acetylcholine did not result from direct activation of endogenous muscarinic receptors since no $G\alpha_{oB}$ response was observed in parental cells. Given that the M_3

muscarinic receptor, which is endogenously expressed at relatively high levels in HEK293 cells (Atwood, Lopez, Wager-Miller, Mackie, & Straiker, 2011), is strongly coupled to the $G_{q/11}$, CB_1-expressing cells were pretreated with $G_{q/11/14}$ inhibitor UBO-QIC prior to stimulation with acetylcholine. UBO-QIC pre-treatment blocked acetylcholine- but not WIN55,212-2-mediated $G\alpha_{oB}$ activation (**Figure 6C**, right). These results demonstrate that CB_1 activation by acetylcholine is indirect and potentially involves the secretion of an endogenous CBR ligand following activation of $G_{q/11}$ by endogenous muscarinic acetylcholine receptors. The combined G_z/G_{15} sensor is therefore a useful tool to identify interplay between receptors and to explore systems pharmacology resulting from such cross-talks.

Discussion

This study describes the development and validation of a platform of genetically encoded ebBRET-based biosensors allowing live-cell mapping of GPCR/G protein coupling preferences covering 12 heterotrimeric G proteins. The novel EMTA biosensors were combined with previously described ebBRET-based βarrestin trafficking sensors (Namkung et al., 2016), providing an unprecedented description of GPCR signaling partner couplings. In addition to providing a resource to study GPCR functional selectivity (see companion paper (Hauser et al., 2021)), the sensors provide versatile and readily usable tools to study, on a large-scale, pharmacological processes such as constitutive activity, inverse agonism, ligand-biased signaling, and signaling cross-talk.

Our EMTA-based biosensor platform offers several advantages relative to other available approaches. First, EMTA provides direct real-time measurement of proximal signaling events following GPCR activation (i.e., Gα protein activation and βarrestin recruitment) and does not require amplification or extended incubation times for signal detection. This contrasts with distal readouts that rely on biological responses that can be modulated by multiple downstream signaling pathways that could engage in cross-talk regulation, complicating data interpretation (Mancini, Frauli, & Breton, 2015).

Second, EMTA uses native untagged GPCRs and G protein subunits, contrary to protein complementation (Laschet, Dupuis, & Hanson, 2019), FRET/BRET-based Gαβγ dissociation/receptor-G protein interaction (Bunemann, Frank, & Lohse, 2003; Gales et al., 2005; Gales et al., 2006; Hoffmann et al., 2005; Namkung et al., 2018; Olsen et al., 2020) or TGF-α shedding (Inoue et al., 2019) assays. Modifying these core-signaling components could alter responses, complicate interpretation and explain some of the discrepancies observed between the EMTA platform and other approaches used to study G protein activation. Moreover, the ability to work with unmodified receptors and G proteins offers numerous advantages. First, it allows for the detection of endogenous GPCR signaling in either generic HEK293 cells (**Figure S5**) or more physiologically relevant

cell lines such as promyelocytic HL-60 cells (**Figure 7A**) and induced pluripotent stem cell (iPSC)-derived cardiomyocytes (**Figure 7B**). Further it allows, in cells expressing sufficient endogenous level of the receptors and G proteins of interest, to detect G protein activation with native components. This is illustrated by the ability to detect the recruitment of Rap1GAP upon activation of the endogenous PAR2 and $G_{i/o}$ family members in HEK293 cells (**Figure 7C**). Recently, another BRET-based approach (Maziarz et al., 2020), taking advantage of a synthetic peptide recognizing the GTP-bound form of Gα subunits, also allows the detection of native G protein activation offering alternative means to probe coupling selectivity profiles for both endogenously expressed and overexpressed GPCRs.

Finally, similarly to BERKY, the EMTA assay platform detects the active form of the Gα subunits rather than the surrogate measurement of Gαβγ dissociation (Gales et al., 2005; Masuho et al., 2015; Maziarz et al., 2020; Mende et al., 2018), which can also detect non-productive engagement as recently described for the V_2 engagement of G_{12} (Okashah et al., 2020).

A potential caveat of EMTA is the use of common downstream effectors for all members of a given G protein family. Indeed, one cannot exclude the distinct members of a given family may display different relative affinities for their common effector. However, such differences are compensated by our data normalization that establishes the maximal response observed for a given subtype as the reference for this pathway (**Figure 3A**). A second potential caveat of EMTA is the use of overexpressed GPCRs and G proteins. Some of the responses detected could indeed result from favorable stoichiometries that may not exist under physiological conditions. It follows that the profiling represents the coupling possibilities of a given GPCR and not necessarily the coupling that will be observed in all cell types.

Because we elected to use unmodified receptors (*i.e.*: not bearing any tags), the expression level of receptors could not be directly monitored. However, the double normalization method developed (see Methods) allows quantitative comparison of coupling preferences across different receptors curtailing the influence of the assay response windows as well receptor expression levels. This method could be used in other comparative studies.

Another limitation is the lack of a soluble effector protein selective for activated $G\alpha_s$ thus requiring tagging of the $G\alpha_s$ subunit (**Figure 1B**, bottom) and monitoring its dissociation from the plasma membrane. Yet, our data show that this translocation reflects G_s activation state, justifying its use in a G protein activation detection platform.

Finally, because EMTA is able to detect constitutive activity, high receptor expression level may lead to an elevated basal signal level that may obscure an agonist-promoted response. Such an example can be appreciated for the A_1 receptor for which the agonist-promoted $G\alpha_{i2}$ response did not reach the activation threshold criteria because of a very high constitutive activity level (**Figure 5A**). The impact of receptor expression on the constitutive activity and the narrowing on the agonist-promoted response is illustrated for $G\alpha_q$ activation by the 5-HT_{2C} (**Figure S9**).

A limitation of any large-scale signaling study and drug discovery program is that ligands may elicit responses downstream of receptors other than the one under study. The development of a G_z/G_{15} quasi-universal biosensor enables efficient screening and detection of such polypharmacology and cross-talk. Using a combination of EMTA and appropriate pharmacological tools, we also proposed a systematic approach to distinguish off-target action of ligands from cross-talk. Interestingly, the cross-talk between the M_3 and CB receptors detected (**Figure 6**) may have physiological relevance since activation of muscarinic acetylcholine receptors has been shown to enhance the release of endocannabinoids in the hippocampus (Kim, Isokawa, Ledent, & Alger, 2002).

The combined G_z/G_{15} biosensor should be particularly useful for early profiling of compound activity on safety panels and for the design of drugs displaying polypharmacology, an approach that is increasingly considered for the development neuropsychiatric drugs (Roth, Sheffler, & Kroeze, 2004).

The EMTA platform undoubtedly represents a novel tool-set that may be used for high throughput screening of small molecules and biologics across an array of signaling pathways, allowing for the discovery of functionally selective molecules or for GPCR deorphanization campaigns. The ability of the EMTA platform to quantitatively assess -G protein coupling selectivity firmly expands the concept of functional selectivity and potential ligand bias beyond the dichotomic G protein *vs.* βarrestin view and provides plausible functional selectivity profiles that could be tested for their biological and pharmacological outcomes.

Materials and Methods

Cells

HEK293 clonal cell line (HEK293SL cells), hereafter referred as HEK293 cells, were a gift from S. Laporte (McGill University, Montreal, Quebec, Canada) and previously described (Namkung et al., 2016). HEK293 cells devoid of functional $G\alpha_s$ (ΔG_s), $G\alpha_{12}$ and $G\alpha_{13}$ ($\Delta G_{12/13}$), $G\alpha_q$, $G\alpha_{11}$, $G\alpha_{14}$ and $G\alpha_{15}$ ($\Delta G_{q/11}$) and, $G\alpha_{i,}$ and $G\alpha_o$ ($\Delta G_{i/o}$) proteins were a gift from Dr. A. Inoue (Tohoku University, Sendai, Miyagi, Japan) and previously described (Devost et al., 2017; Namkung et al., 2018; Schrage et al., 2015; Stallaert et al., 2017). Cells were maintained in Dulbecco's Modified Eagle Medium (DMEM, Wisent, Saint-Jean-Baptiste, QC, Canada) supplemented with 10% fetal bovine serum (FBS, Wisent) and 1% antibiotics (100 U/mL penicillin and 100 µg/mL streptomycin (PS); Wisent). Cells were grown at 37°C in 5% CO_2 and 90% humidity.

Plasmids and ebBRET biosensor constructs

Only human GPCRs and human Gα subunits were used in this study. An open reading frame of each full-length GPCR was cloned into pcDNA3.1(+) expression plasmid. Except when otherwise specified, GPCRs sequences were devoid of epitope tags.

$G\alpha_s$-67-RlucII (Carr et al., 2014), βarrestin1-RlucII (Zimmerman et al., 2012), βarrestin2-RlucII (Quoyer et al., 2013), rGFP-CAAX (Namkung et al., 2016), EPAC (Leduc et al., 2009), PKN-RBD-RlucII (Namkung et al., 2018), HA-β_2AR (Lavoie et al., 2002), signal peptide-Flag-AT_1 (Goupil et al., 2015) and EAAC-1 (Brabet et al., 1998) were previously described. Full-length, untagged Gα subunits, $G\beta_1$ and $G\gamma_9$ were purchased from cDNA Resource Center. GRK2 was generously provided by Dr. Antonio De Blasi (Istituto Neurologico Mediterraneo Neuromed, Pozzilli, Italy).

To selectively detect $G_{i/o}$ activation, a construct coding for aa 1-442 of Rap1 GTPase-activating protein (comprising a $G_{i/o}$ binding domain) fused to Rluc8, was sequence-optimized, synthetized and subcloned at TopGenetech (St-Laurent, QC, Canada). From this construct, a RlucII tagged version of Rap1GAP (1-442) with a linker sequence

(GSAGTGGRAIDIKLPAT) between Rap1GAP and RlucII was created by Gibson assembly in pCDNA3.1_Hygro (+) GFP10-RlucII, replacing GFP10. Three substitutions (i.e., S437A/S439A/S441A) were introduced into the Rap1GAP sequence by PCR-mediated mutagenesis. These putative (S437 and S439) and documented (S441) (McAvoy, Zhou, Greengard, & Nairn, 2009) protein kinase A phosphorylation sites were removed in order to eliminate any G_s-mediated Rap1GAP recruitment to the plasma-membrane.

To selectively detect $G_{q/11}$ activation, a construct encoding the G_q binding domain of the human p63 Rho guanine nucleotide exchange factor (p63RhoGEF; residues: 295-502) tagged with RlucII was done from IMAGE clones (OpenBiosystems; Burlington, ON, Canada) and subcloned by Gibson assembly in pCDNA3.1_Hygro (+) GFP10-RlucII, replacing GFP10. The G_q binding domain of p63RhoGEF and RlucII were separated by the peptidic linker ASGSAGTGGRAIDIKLPAT.

To selectively detect $G_{12/13}$ activation, a construct encoding the $G_{12/13}$ binding domain of the human PDZ-RhoGEF (residues: 281-483) tagged with RlucII was done by PCR amplification from IMAGE clones (OpenBiosystems) and subcloned by Gibson assembly in pCDNA3.1_Hygro (+) GFP10-RlucII, replacing GFP10. The peptidic linker GIRLREALKLPAT is present between RlucII and the $G_{12/13}$ binding domain of PDZ-RhoGEF.

Transfection

For BRET experiments, cells (1.2 mL at 3.5×10^5 cells per mL) were transfected with a fixed final amount of pre-mixed biosensor-encoding DNA (0.57 µg, adjusted with salmon sperm DNA; Invitrogen) and human receptor DNA. Transfections were performed using a polyethylenimine solution (PEI, 1 mg/mL; Polysciences, Warrington, PA, USA) diluted in NaCl (150 mM, pH 7.0; 3:1 PEI/DNA ratio). Gelatin solution (1%; Sigma-Aldrich, Saint-Louis, Missouri) was used to stabilize DNA/PEI transfection mixes. Following addition of cells to the stabilized DNA/PEI transfection mix, cells were immediately seeded (3.5×10^4 cells/well) into 96-well white microplates (Greiner Bio-one; Monroe, NC, USA) and maintained in culture for the next 48 h in DMEM containing 2% FBS and 1% PS. DMEM

480 medium without L-glutamine (Wisent) was used for transfection of cells with mGluR to
481 avoid receptor activation and desensitization.
482 For Ca^{2+} experiments, cells (3.5 x 10^4 cells/well) were co-transfected with the indicated
483 receptor, with or without $G\alpha_{15}$ protein, using PEI and seeded in poly-ornithine coated 96-
484 well clear-bottomed black microplates (Greiner Bio-one) and maintained in culture for
485 the next 48 h.
486 For BRET-based imagery, cells (4 x 10^5 cells/dish) were seeded into 35-mm poly-d-lysine-
487 coated glass-bottom culture dishes (Mattek Corporation; Ashland, MA, USA) in 2 ml of
488 fresh medium and incubated at 37°C in 5% CO_2, 3 day before imaging experiments.
489 Twenty-four hours later, cells were transfected with EMTA ebBRET biosensors and the
490 indicated receptor (i.e., p63-RhoGEF-RlucII/rGFP-CAAX + $G\alpha_q$ and GnRHR, Rap1GAP-
491 RlucII/rGFP-CAAX + $G\alpha_{i2}$ and D_2 or PDZ-RhoGEF-RlucII/rGFP-CAAX + $G\alpha_{13}$ and TPαR) using
492 X-tremeGENE 9 DNA transfection reagent (3:1 reagent/DNA ratio; Roche) diluted in
493 OptiMEM (Gibco) and maintained in culture for the next 48 h in DMEM containing 10%
494 FBS and 1% PS.
495
496 **Bioluminescence Resonance Energy Transfer Measurement**
497 Enhanced bystander BRET (ebBRET) was used to monitor the activation of each Gα
498 protein, as well as βarrestin 1 and 2 recruitment to the plasma membrane. $G\alpha_s$ protein
499 engagement was measured between the plasma membrane marker rGFP-CAAX and
500 human $G\alpha_s$-RlucII in presence of human $G\beta_1$, $G\gamma_9$ and the tested receptor. $G\alpha_s$
501 downstream cAMP production was determined using the EPAC biosensor and GPBA
502 receptor. $G\alpha_{i/o}$ protein family activation was followed using the selective-$G_{i/o}$ effector
503 Rap1GAP-RlucII and rGFP-CAAX along with the human $G\alpha_{i1}$, $G\alpha_{i2}$, $G\alpha_{oA}$, $G\alpha_{oB}$ or $G\alpha_z$
504 subunits and the tested receptor. $G\alpha_{q/11}$ protein family activation was determined using
505 the selective-$G_{q/11}$ effector p63-RhoGEF-RlucII and rGFP-CAAX along with the human $G\alpha_q$,
506 $G\alpha_{11}$, $G\alpha_{14}$ or $G\alpha_{15/16}$ subunits and the tested receptor. $G\alpha_{12/13}$ protein family activation
507 was monitored using the selective-$G_{12/13}$ effector PDZ-RhoGEF-RlucII and rGFP-CAAX in
508 presence of either $G\alpha_{12}$ or $G\alpha_{13}$ and the tested receptor. The expression level of the Gα

subunits was monitored by Western blot in HEK293 cells that endogenously expressed $G\alpha_{i1}$, $G\alpha_{i2}$, $G\alpha_{12}$, $G\alpha_{13}$, $G\alpha_{q}$, $G\alpha_{11}$, $G\alpha_{14}$ and $G\alpha s$ but not $G\alpha_{oA}$, $G\alpha_{oB}$, $G\alpha_{z}$ and $G\alpha_{15}$ (**Figure S10**). $G\alpha_{12/13}$-downstream activation of the Rho pathway was measured using PKN-RBD-RlucII and rGFP-CAAX with the indicated receptor. βarrestin recruitment to the plasma membrane was determined using DNA mix containing rGFP-CAAX and βarrestin1-RlucII with GRK2 or βarrestin2-RlucII alone or with GRK2 and the tested receptor. Glutamate transporters EAAC-1 and EAAT-1 were systematically co-transfected with the mGluR to prevent receptor activation and desensitization by glutamate secreted in the medium by the cells (Brabet et al., 1998). All ligands were also tested for potential activation of endogenous receptors by transfecting the biosensors without receptor DNA. The G_z/G_{15} biosensor consists of a combination of the following plasmids: rGFP-CAAX, Rap1GAP-RlucII, $G\alpha_{z}$, p63-RhoGEF-RlucII and $G\alpha_{15}$.

The day of the BRET experiment, cells were incubated in HBSS for 1 h at room temperature (RT). Cells were then co-treated with increasing concentrations of ligand (see **Supplementary Table 2** for details) and the luciferase substrate coelenterazine prolume purple (1 µM, NanoLight Technologies; Pinetop, AZ, USA) for 10 min at RT. Plates were read on a Synergy Neo microplate reader (BioTek Instruments, Inc.; Winooski, VT, USA) equipped with 410 ± 80 nm donor and 515 ± 30 nm acceptor filters or with a Spark microplate reader (Tecan; Männedorf, Switzerland) using the $BRET^2$ manufacturer settings. The BRET signal ($BRET^2$) was determined by calculating the ratio of the light intensity emitted by the acceptor over the light intensity emitted by the donor. To validate the specificity of the biosensor responses, cells were pretreated in the absence or presence of either the $G\alpha_{q}$ inhibitor UBO-QIC (100 nM, 30 min; Institute for Pharmaceutical Biology of the University of Bonn, Germany), the $G\alpha_{i/o}$ inhibitor PTX (100 ng/mL, 18 h; List Biological Laboratories, Campbell, California, USA) or the $G\alpha_{s}$ activator CTX (0 to 200 ng/mL, 4h; Sigma-Aldrich) before stimulation with agonist. For ligand-cross receptor activation experiments, cells were pretreated for 10 min with increasing concentrations of antagonists or inverse agonist (eticlopride for D_2, WB4101 for $\alpha_{2A}AR$,

atropine for muscarinic receptors and AM-630 for CB_1) before a 10 min stimulation with an EC_{80} concentration of the indicated agonist. BRET was measured as described above. For the safety target panel ligand screen using the combined G_z/G_{15} sensor, basal ebBRET level was first measured 10 min following addition of coelenterazine prolume purple (1 µM) and ebBRET level was measured again following a 10 min stimulation with a single dose of the indicated ligand (1 µM for endothelin-1 and 10 µM for all other ligands). Technical replicates for each receptor were included on the same 96-well plate. For kinetics experiment of ET_A activation, basal BRET was measured during 150 sec before cells stimulation with either vehicle (DMSO) or 1 µM of endothelin-1 (at time 0 sec) and BRET signal was recorded each 30 sec during 3570 sec. For the validation of $G_{12/13}$-mediated signal by new identified $G_{12/13}$-coupled receptor using RhoA activation sensor, cells were pretreated or not with the $G\alpha_q$ inhibitor YM-254890 (1 µM, 30 min; Wako Pure Chemical Industries; Wako Pure Chemical Industries (Fujifilm), Osaka, Japan) before agonist stimulation for 10 min.

BRET Data analyses and coupling efficiency evaluation

All BRET ratios were standardized using the equation below and represented as universal BRET (*u*BRET) values: *u*BRET = ((BRET ratio – A)/(B-A)) * 10 000. Constants A and B correspond to the following values:

A = pre-established BRET ratio obtained from transfection of negative control (vector coding for RlucII alone);

B = pre-established BRET ratio obtained from transfection of positive control (vector coding for a GFP10-RlucII fusion protein).

For a given signaling pathway, *u*BRET values at each agonist concentration were normalized as the % of the response obtained in the absence of agonist (vehicle) and concentration-response curves were fitted in GraphPad Prism 8 software using a four-parameter logistic nonlinear regression model. Results are expressed as mean ± SEM of at least three independent experiments.

A ligand-promoted response was considered real when the E_{max} value was ≥ to the mean + 2*SD of the response obtained in vehicle condition and that a pEC_{50} value could be determined in the agonist concentration range used to stimulate the receptor. Consequently, a score of 0 or 1 was assigned to each signaling pathway depending on an agonist's ability to activate the tested pathway (0= no activation; 1= activation). In the case were responses associated to endogenous receptor were detectable, we considered as "distorted" and exclude all the responses observed in the presence of transfected receptor for which E_{max} was ≤ to 2*mean of the E_{max} value obtained with endogenous receptors or pEC_{50} was ≥ to 2*mean of the pEC_{50} value obtained with endogenous receptors. Consequently, a score of 0 was assigned for these distorted responses in radial graph representation (**Figure S4**) and dose-response curves were placed on a gray background in signaling signature profile panels (**Supplementary File 1**). Whenever transfected receptors produced an increase in E_{max} or a left-shift in pEC_{50} values compared to endogenous receptors, responses were considered 'true' and were assigned with a score of 1 for radial graph representation (**Figure S4**) and dose-response curves were placed on a yellow background in signaling signature profile panels to indicate a partial contribution of endogenous receptors (**Supplementary File 1**).

We used a double normalization of E_{max} and pEC_{50} values to compare the signaling efficiency obtained for the 100 GPCRs across all receptors and pathways. E_{max} and pEC_{50} values deduced from concentration-response curves were first normalized between 0 and 1 across receptors by ranking the receptors as a function of the receptor that most efficiently activate a given pathway and then using the activation value for the pathway (including G protein and βarrestin subtypes) that a given receptor most efficiently activate as a reference for the other pathways that can be activated by this receptor. This double normalization can be translated in the following formalized equation:

- STEP1: For each receptor and for each pathway:

$\left[\frac{E_{max}\ GPCR_x}{E_{max}\ GPCR_{Ref}}\right]_{Pathway\ A}$ = *Pathway specific normalized score for GPCR$_x$ on pathway A ([PSNS GPCR$_x$]$_{Pathway\ A}$)*

Where: $GPCR_x$ is receptor being analyzed, $GPCR_{Ref}$ is the receptor giving greatest E_{max} on pathway A of all receptors studied (i.e., reference receptor for pathway A). A PSNS was determined for every receptor and every pathway coupled to that receptor.

- STEP2: For any given receptor:

$$\frac{[PSNS\ GPCR_x]_{\ Pathway\ A}}{[PSNS\ GPCR_x]_{\ Ref\ pathway}} = \textit{Normalized pathway A coupling score for GPCR}_x$$

Where: $[PSNS\ GPCR_x]_{\ Pathway\ A}$ is the pathway specific normalized score for $GPCR_x$ on pathway A, and $[PSNS\ GPCR_x]_{\ Ref\ pathway}$ is the pathway specific normalized score for the pathway giving the highest PSNS for $GPCR_x$ (i.e., reference pathway for $GPCR_x$).

For the safety target panel ligand screen using the combined G_z/G_{15} sensor, the fold ligand-induced stimulation was calculated for each receptor by dividing the BRET ratio after ligand addition (measured at 10 minutes post stimulation) by the basal BRET ratio prior to receptor stimulation. Activation thresholds were defined as the mean + 2*SD of the ligand-stimulated response obtained with receptor-null cells expressing only the combined G_z/G_{15} sensor.

Ca^{2+} mobilization assay

The day of experiment, cells were incubated with 100 µL of a Ca^{2+}-sensitive dye-loading buffer (FLIPR calcium 5 assay kit, Molecular Devices; Sunnyvale, CA, USA) containing 2.5 mM probenecid (Sigma-Aldrich) for 1 h at 37°C in a 5% CO_2 incubator. During a data run, cells in individual wells were exposed to an EC_{80} concentration of agonist, and fluorescent signals were recorded every 1.5 s for 3 min using the FlexStation II microplate reader (Molecular Devices). For receptors that also activate other $G_{q/11}$ family members, cells were pretreated with the $G_{q/11}$ inhibitor YM-254890 (1 µM, 30 min) before agonist

stimulation. $G\alpha_{15}$ is resistant to inhibition by YM-254890, thus allowing to measure Ca^{2+} responses generated specifically by $G\alpha_{15}$.

BRET-based imaging

BRET images were obtained as previously described (Kobayashi, Picard, Schonegge, & Bouvier, 2019). Briefly, the day of imaging experiment, cells were carefully rinsed with HBSS, and images were acquired before and after agonists addition (100 nM for GnRH and U46619, and 1 µM for dopamine) diluted in HBSS in presence of the luciferase substrate coelenterazine prolume purple (20 µM).

Images were recorded using an inverted microscope (Nikon Eclipse Ti-U) equipped with x60 objective lens (Nikon CFI Apochromat TIRF) and EM-CCD camera (Nuvu HNu 512). Measurements were carried out in photon counting mode with EM gain 3,000. Exposure time of each photon counting was 100 ms. Successive 100 frames were acquired alternatively with 480 nm longpass filter (acceptor frames) or without filter (total luminescence frames), and integrated. Image integrations were repeated 5 times and 500 frames of acceptor and total luminescence were used to generate each image.

BRET values were obtained by dividing acceptor counts by total luminescence counts pixelwise. BRET values from 0.0 to 0.5 were allocated to 'jet' heatmap array using MATLAB 2019b. Brightness of each pixel was mapped from the signal level of total luminescence image. 0% and 99.9% signal strength were allocated to the lowest and highest brightness to exclude the influence of defective pixels with gamma correction factor of 2.0.

The movie was generated using ImageJ 1.52a. Frame rate is 3 frames/sec, and frame interval is 100 sec. The field of view of the movie is 137 um x 137 um.

Western blot analysis

Cells were transfected or not with the indicated biosensors mix as previously described and whole-cell extracts were prepared 48 h later. Briefly, cells were washed with ice-cold PBS and lysed in a buffer containing 10 mM Tris buffer (pH 7.4), 100 mM NaCl, 1 mM EDTA, 1 mM EGTA, 0.1% SDS, 1% Triton X-100, 10% Glycerol supplemented with protease

652 inhibitors cocktails (Thermo Fisher Scientific). Cell lysates were centrifuged at 13,000 × g
653 for 30 min at 4°C. Equal amounts of proteins were separated by SDS-PAGE and transferred
654 onto polyvinylidene fluoride membrane. The membranes were blocked in (incubation 1
655 hr at room temperature in PBS 0.1% Tween-20, 5% BSA) and successively probed with
656 primary antibody and appropriate goat secondary antibodies coupled to horseradish
657 peroxidase (described in table below). Western blots were visualized using enhanced
658 chemiluminescence and detection was performed using a ChemiDoc MP Imaging System
659 (BioRad). Relative densitometry analysis on protein bands was performed using
660 MultiGauge software (Fujifilm). Results were normalized against control bands.
661

Target	**Dilution**	**Species**	**Class**	**Reference**	**Manufacturer**
Gαi1 (I-20)	1:500	Rabbit	polyclonal	#sc-391	Santa Cruz
Gαi2 (T-19)	1:500	Rabbit	polyclonal	#sc-7276	Santa Cruz
Gαo (K-20)	1:500	Rabbit	polyclonal	#sc-387	Santa Cruz
Gαz	1:1,000	Rabbit	monoclonal	# ab154846	Abcam
Gαs (K-20)	1:500	Rabbit	polyclonal	#sc-823	Santa Cruz
Gα12 (S-20)	1:500	Rabbit	polyclonal	#sc-409	Santa Cruz
Gα13 (A-20)	1:500	Rabbit	polyclonal	#sc-410	Santa Cruz
Gαq (E-17)	1:500	Rabbit	polyclonal	#sc-393	Santa Cruz
Gα11 (C-terminal)	1:500	Rabbit	Polyclonal	#SAB2109181	Sigma-Aldrich
Gα14	1:500	Rabbit	Polyclonal	#SAB4300771	Sigma-Aldrich
Gα15	1:5,000	Rabbit	Polyclonal	#PA1-29022	ThermoFisher scientific (Pierce)
βactin	1:5,000	Mouse	Monoclonal	#A5441	Sigma-Aldrich
Anti-rabbit HRP-coupled	1:5,000	Donkey	Polyclonal	#NA934	GE Healthcare
Anti-mouse HRP-coupled	1:10,000	Sheep	Polyclonal	#NA931	GE Healthcare

662

663 **Statistical Analyses**

664 Curve fitting and statistical analyses were performed using GraphPad Prism 8.3 software
665 and methods are described in the legends of the figures. Significance was determined as
666 $p < 0.05$.

References

Atwood, B. K., Lopez, J., Wager-Miller, J., Mackie, K., & Straiker, A. (2011). Expression of G protein-coupled receptors and related proteins in HEK293, AtT20, BV2, and N18 cell lines as revealed by microarray analysis. *BMC Genomics, 12*, 14. doi:10.1186/1471-2164-12-14

Azzi, M., Charest, P. G., Angers, S., Rousseau, G., Kohout, T., Bouvier, M., & Pineyro, G. (2003). Beta-arrestin-mediated activation of MAPK by inverse agonists reveals distinct active conformations for G protein-coupled receptors. *Proc Natl Acad Sci U S A, 100*(20), 11406-11411. doi:10.1073/pnas.1936664100

Bowes, J., Brown, A. J., Hamon, J., Jarolimek, W., Sridhar, A., Waldron, G., & Whitebread, S. (2012). Reducing safety-related drug attrition: the use of in vitro pharmacological profiling. *Nat Rev Drug Discov, 11*(12), 909-922. doi:10.1038/nrd3845

Brabet, I., Parmentier, M. L., De Colle, C., Bockaert, J., Acher, F., & Pin, J. P. (1998). Comparative effect of L-CCG-I, DCG-IV and gamma-carboxy-L-glutamate on all cloned metabotropic glutamate receptor subtypes. *Neuropharmacology, 37*(8), 1043-1051. doi:10.1016/s0028-3908(98)00091-4

Bunemann, M., Frank, M., & Lohse, M. J. (2003). Gi protein activation in intact cells involves subunit rearrangement rather than dissociation. *Proc Natl Acad Sci U S A, 100*(26), 16077-16082. doi:10.1073/pnas.2536719100

Carr, R., 3rd, Du, Y., Quoyer, J., Panettieri, R. A., Jr., Janz, J. M., Bouvier, M., . . . Benovic, J. L. (2014). Development and characterization of pepducins as Gs-biased allosteric agonists. *J Biol Chem, 289*(52), 35668-35684. doi:10.1074/jbc.M114.618819

Casey, P. J., Fong, H. K., Simon, M. I., & Gilman, A. G. (1990). Gz, a guanine nucleotide-binding protein with unique biochemical properties. *J Biol Chem, 265*(4), 2383-2390. Retrieved from https://www.ncbi.nlm.nih.gov/pubmed/2105321

De Haan, L., & Hirst, T. R. (2004). Cholera toxin: a paradigm for multi-functional engagement of cellular mechanisms (Review). *Mol Membr Biol, 21*(2), 77-92. doi:10.1080/09687680410001663267

Devost, D., Sleno, R., Petrin, D., Zhang, A., Shinjo, Y., Okde, R., . . . Hebert, T. E. (2017). Conformational Profiling of the AT1 Angiotensin II Receptor Reflects Biased Agonism, G Protein Coupling, and Cellular Context. *J Biol Chem, 292*(13), 5443-5456. doi:10.1074/jbc.M116.763854

Fukuhara, S., Chikumi, H., & Gutkind, J. S. (2001). RGS-containing RhoGEFs: the missing link between transforming G proteins and Rho? *Oncogene, 20*(13), 1661-1668. doi:10.1038/sj.onc.1204182

Galandrin, S., Oligny-Longpre, G., & Bouvier, M. (2007). The evasive nature of drug efficacy: implications for drug discovery. *Trends Pharmacol Sci, 28*(8), 423-430. doi:10.1016/j.tips.2007.06.005

Gales, C., Rebois, R. V., Hogue, M., Trieu, P., Breit, A., Hebert, T. E., & Bouvier, M. (2005). Real-time monitoring of receptor and G-protein interactions in living cells. *Nat Methods, 2*(3), 177-184. doi:10.1038/nmeth743

Gales, C., Van Durm, J. J., Schaak, S., Pontier, S., Percherancier, Y., Audet, M., . . . Bouvier, M. (2006). Probing the activation-promoted structural rearrangements in preassembled receptor-G protein complexes. *Nat Struct Mol Biol, 13*(9), 778-786. doi:10.1038/nsmb1134

Goupil, E., Fillion, D., Clement, S., Luo, X., Devost, D., Sleno, R., . . . Hebert, T. E. (2015). Angiotensin II type I and prostaglandin F2alpha receptors cooperatively modulate signaling in vascular smooth muscle cells. *J Biol Chem, 290*(5), 3137-3148. doi:10.1074/jbc.M114.631119

Hauser, A. S., Attwood, M. M., Rask-Andersen, M., Schioth, H. B., & Gloriam, D. E. (2017). Trends in GPCR drug discovery: new agents, targets and indications. *Nat Rev Drug Discov, 16*(12), 829-842. doi:10.1038/nrd.2017.178

Hauser, A. S., Avet, C., Normand, C., Mancini, A., Inoue, A., Bouvier, M., & Gloriam, D. E. (2021). GPCR-G protein selectivity - a unified meta-analysis *bioRxiv*. doi:https://doi.org/10.1101/2021.09.07.459250

Hoffmann, C., Gaietta, G., Bunemann, M., Adams, S. R., Oberdorff-Maass, S., Behr, B., . . . Lohse, M. J. (2005). A FlAsH-based FRET approach to determine G protein-coupled receptor activation in living cells. *Nat Methods, 2*(3), 171-176. doi:10.1038/nmeth742

Inoue, A., Raimondi, F., Kadji, F. M. N., Singh, G., Kishi, T., Uwamizu, A., . . . Russell, R. B. (2019). Illuminating G-Protein-Coupling Selectivity of GPCRs. *Cell, 177*(7), 1933-1947 e1925. doi:10.1016/j.cell.2019.04.044

720 Jordan, J. D., Carey, K. D., Stork, P. J., & Iyengar, R. (1999). Modulation of rap activity by direct interaction
721 of Galpha(o) with Rap1 GTPase-activating protein. *J Biol Chem, 274*(31), 21507-21510.
722 doi:10.1074/jbc.274.31.21507
723 Kawamata, Y., Fujii, R., Hosoya, M., Harada, M., Yoshida, H., Miwa, M., . . . Fujino, M. (2003). A G protein-
724 coupled receptor responsive to bile acids. *J Biol Chem, 278*(11), 9435-9440.
725 doi:10.1074/jbc.M209706200
726 Kenakin, T. (2019). Biased Receptor Signaling in Drug Discovery. *Pharmacol Rev, 71*(2), 267-315.
727 doi:10.1124/pr.118.016790
728 Kim, J., Isokawa, M., Ledent, C., & Alger, B. E. (2002). Activation of muscarinic acetylcholine receptors
729 enhances the release of endogenous cannabinoids in the hippocampus. *J Neurosci, 22*(23), 10182-
730 10191. Retrieved from https://www.ncbi.nlm.nih.gov/pubmed/12451119
731 Kobayashi, H., Picard, L. P., Schonegge, A. M., & Bouvier, M. (2019). Bioluminescence resonance energy
732 transfer-based imaging of protein-protein interactions in living cells. *Nat Protoc, 14*(4), 1084-1107.
733 doi:10.1038/s41596-019-0129-7
734 Laschet, C., Dupuis, N., & Hanson, J. (2019). A dynamic and screening-compatible nanoluciferase-based
735 complementation assay enables profiling of individual GPCR-G protein interactions. *J Biol Chem,*
736 *294*(11), 4079-4090. doi:10.1074/jbc.RA118.006231
737 Lavoie, C., Mercier, J. F., Salahpour, A., Umapathy, D., Breit, A., Villeneuve, L. R., . . . Hebert, T. E. (2002).
738 Beta 1/beta 2-adrenergic receptor heterodimerization regulates beta 2-adrenergic receptor
739 internalization and ERK signaling efficacy. *J Biol Chem, 277*(38), 35402-35410.
740 doi:10.1074/jbc.M204163200
741 Leduc, M., Breton, B., Gales, C., Le Gouill, C., Bouvier, M., Chemtob, S., & Heveker, N. (2009). Functional
742 selectivity of natural and synthetic prostaglandin EP4 receptor ligands. *J Pharmacol Exp Ther,*
743 *331*(1), 297-307. doi:10.1124/jpet.109.156398
744 Lu, M., Wang, B., Zhang, C., Zhuang, X., Yuan, M., Wang, H., . . . Li, J. (2014). PQ-69, a novel and selective
745 adenosine A1 receptor antagonist with inverse agonist activity. *Purinergic Signal, 10*(4), 619-629.
746 doi:10.1007/s11302-014-9424-5
747 Lutz, S., Shankaranarayanan, A., Coco, C., Ridilla, M., Nance, M. R., Vettel, C., . . . Tesmer, J. J. (2007).
748 Structure of Galphaq-p63RhoGEF-RhoA complex reveals a pathway for the activation of RhoA by
749 GPCRs. *Science, 318*(5858), 1923-1927. doi:10.1126/science.1147554
750 Mancini, A., Frauli, M., & Breton, B. (2015). Exploring the Technology Landscape of 7TMR Drug Signaling
751 Profiling. *Curr Top Med Chem, 15*(24), 2528-2542. doi:10.2174/1568026615666150701113344
752 Martin, B. R., & Lambert, N. A. (2016). Activated G Protein Galphas Samples Multiple Endomembrane
753 Compartments. *J Biol Chem, 291*(39), 20295-20302. doi:10.1074/jbc.M116.729731
754 Masuho, I., Ostrovskaya, O., Kramer, G. M., Jones, C. D., Xie, K., & Martemyanov, K. A. (2015). Distinct
755 profiles of functional discrimination among G proteins determine the actions of G protein-coupled
756 receptors. *Sci Signal, 8*(405), ra123. doi:10.1126/scisignal.aab4068
757 Maziarz, M., Park, J. C., Leyme, A., Marivin, A., Garcia-Lopez, A., Patel, P. P., & Garcia-Marcos, M. (2020).
758 Revealing the Activity of Trimeric G-proteins in Live Cells with a Versatile Biosensor Design. *Cell,*
759 *182*(3), 770-785 e716. doi:10.1016/j.cell.2020.06.020
760 McAvoy, T., Zhou, M. M., Greengard, P., & Nairn, A. C. (2009). Phosphorylation of Rap1GAP, a striatally
761 enriched protein, by protein kinase A controls Rap1 activity and dendritic spine morphology. *Proc*
762 *Natl Acad Sci U S A, 106*(9), 3531-3536. doi:10.1073/pnas.0813263106
763 Mende, F., Hundahl, C., Plouffe, B., Skov, L. J., Sivertsen, B., Madsen, A. N., . . . Holst, B. (2018).
764 Translating biased signaling in the ghrelin receptor system into differential in vivo functions. *Proc*
765 *Natl Acad Sci U S A, 115*(43), E10255-E10264. doi:10.1073/pnas.1804003115
766 Meng, J., Glick, J. L., Polakis, P., & Casey, P. J. (1999). Functional interaction between Galpha(z) and
767 Rap1GAP suggests a novel form of cellular cross-talk. *J Biol Chem, 274*(51), 36663-36669.
768 doi:10.1074/jbc.274.51.36663
769 Namkung, Y., Le Gouill, C., Lukashova, V., Kobayashi, H., Hogue, M., Khoury, E., . . . Laporte, S. A.
770 (2016). Monitoring G protein-coupled receptor and beta-arrestin trafficking in live cells using
771 enhanced bystander BRET. *Nat Commun, 7*, 12178. doi:10.1038/ncomms12178
772 Namkung, Y., LeGouill, C., Kumar, S., Cao, Y., Teixeira, L. B., Lukasheva, V., . . . Laporte, S. A. (2018).
773 Functional selectivity profiling of the angiotensin II type 1 receptor using pathway-wide BRET
774 signaling sensors. *Sci Signal, 11*(559). doi:10.1126/scisignal.aat1631

775 Okashah, N., Wright, S. C., Kawakami, K., Mathiasen, S., Zhou, J., Lu, S., . . . Lambert, N. A. (2020).
776 Agonist-induced formation of unproductive receptor-G12 complexes. *Proc Natl Acad Sci U S A, 117*(35), 21723-21730. doi:10.1073/pnas.2003787117
778 Oldham, W. M., & Hamm, H. E. (2008). Heterotrimeric G protein activation by G-protein-coupled receptors.
779 *Nat Rev Mol Cell Biol, 9*(1), 60-71. doi:10.1038/nrm2299
780 Olsen, R. H. J., DiBerto, J. F., English, J. G., Glaudin, A. M., Krumm, B. E., Slocum, S. T., . . . Strachan, R.
781 T. (2020). TRUPATH, an open-source biosensor platform for interrogating the GPCR
782 transducerome. *Nat Chem Biol, 16*(8), 841-849. doi:10.1038/s41589-020-0535-8
783 Quoyer, J., Janz, J. M., Luo, J., Ren, Y., Armando, S., Lukashova, V., . . . Bouvier, M. (2013). Pepducin
784 targeting the C-X-C chemokine receptor type 4 acts as a biased agonist favoring activation of the
785 inhibitory G protein. *Proc Natl Acad Sci U S A, 110*(52), E5088-5097.
786 doi:10.1073/pnas.1312515110
787 Rojas, R. J., Yohe, M. E., Gershburg, S., Kawano, T., Kozasa, T., & Sondek, J. (2007). Galphaq directly
788 activates p63RhoGEF and Trio via a conserved extension of the Dbl homology-associated pleckstrin
789 homology domain. *J Biol Chem, 282*(40), 29201-29210. doi:10.1074/jbc.M703458200
790 Roth, B. L., Sheffler, D. J., & Kroeze, W. K. (2004). Magic shotguns versus magic bullets: selectively non-
791 selective drugs for mood disorders and schizophrenia. *Nat Rev Drug Discov, 3*(4), 353-359.
792 doi:10.1038/nrd1346
793 Schrage, R., Schmitz, A. L., Gaffal, E., Annala, S., Kehraus, S., Wenzel, D., . . . Kostenis, E. (2015). The
794 experimental power of FR900359 to study Gq-regulated biological processes. *Nat Commun, 6*,
795 10156. doi:10.1038/ncomms10156
796 Stallaert, W., van der Westhuizen, E. T., Schonegge, A. M., Plouffe, B., Hogue, M., Lukashova, V., . . .
797 Bouvier, M. (2017). Purinergic Receptor Transactivation by the beta2-Adrenergic Receptor
798 Increases Intracellular Ca(2+) in Nonexcitable Cells. *Mol Pharmacol, 91*(5), 533-544.
799 doi:10.1124/mol.116.106419
800 Takasaki, J., Saito, T., Taniguchi, M., Kawasaki, T., Moritani, Y., Hayashi, K., & Kobori, M. (2004). A novel
801 Galphaq/11-selective inhibitor. *J Biol Chem, 279*(46), 47438-47445. doi:10.1074/jbc.M408846200
802 Wedegaertner, P. B., Bourne, H. R., & von Zastrow, M. (1996). Activation-induced subcellular redistribution
803 of Gs alpha. *Mol Biol Cell, 7*(8), 1225-1233. doi:10.1091/mbc.7.8.1225
804 Wei, H., Ahn, S., Shenoy, S. K., Karnik, S. S., Hunyady, L., Luttrell, L. M., & Lefkowitz, R. J. (2003).
805 Independent beta-arrestin 2 and G protein-mediated pathways for angiotensin II activation of
806 extracellular signal-regulated kinases 1 and 2. *Proc Natl Acad Sci U S A, 100*(19), 10782-10787.
807 doi:10.1073/pnas.1834556100
808 Zimmerman, B., Beautrait, A., Aguila, B., Charles, R., Escher, E., Claing, A., . . . Laporte, S. A. (2012).
809 Differential beta-arrestin-dependent conformational signaling and cellular responses revealed by
810 angiotensin analogs. *Sci Signal, 5*(221), ra33. doi:10.1126/scisignal.2002522

Acknowledgments

We thank Monique Lagacé for critical reading of the manuscript. The authors are grateful to the funding from Bristol-Myers Squibb that supported the detection of Gα proteins by endogenous receptors in iPSC cardiomyocytes and promyelocytic HL-60 cells.

Funding

Canada Research Chair in Signal Transduction and Molecular Pharmacology (MB)

Canadian Institutes of Health Research grant FDN-148431 (MB)

Lundbeck Foundation grants R218-2016-1266 and R313-2019-526 (DEG)

Novo Nordisk Foundation grant NNF18OC0031226 (DEG)

Author contributions

Conceptualization: CA, AM, BB, CLG, XL, MB

Methodology: CA, AM, BB, CLG, MB

Investigation: CA, AM, BB, CN, HK, FG, MH, VL, SS-O, MC, MH, SM

Formal Analysis: CA, AM, ASH, DEG, MB

Resources: AM, EF, J-PF, SS, XL, MB

Supervision: MH, XL, DEG, MB

Funding Acquisition: SS, DEG, MB

Writing: CA, AM, DEG, MB; All coauthors revised the manuscript

Competing interests

AM, BB, CN, FG and SM were employees of Domain Therapeutics North America during part or all of this research.

EF and J-FF are employees and shareholders of Pfizer.

SS and XL are employees and are part of the management of Domain Therapeutics.

MB is the president of Domain Therapeutics scientific advisory board.

BB, CLG, HK, MH, VL, MB have filed patent applications related to the biosensors used in this work and the technology has been licensed to Domain Therapeutics.

CA, ASH, SS-O, MC, MH and DEG have no competing interests to declare.

Data and materials availability

Further information and requests for resources and reagents should be directed to and will be fulfilled upon reasonable request by the Lead Contact, Michel Bouvier (michel.bouvier@umontreal.ca).

The ebBRET sensors used in the study are protected by patent applications and have been licensed to Domain Therapeutics. Inquiries for potential commercial use should be addressed to: xleroy@domaintherapeutics.com. For non-commercial academic use, the sensors can be obtained freely under material transfer agreement upon request to: michel.bouvier@umontreal.ca.

Heatmaps in **Figure 3** were generated using custom python scripts. Scripts are available from the co-corresponding author, David E. Gloriam (david.gloriam@sund.ku.dk) on request.

FIGURES

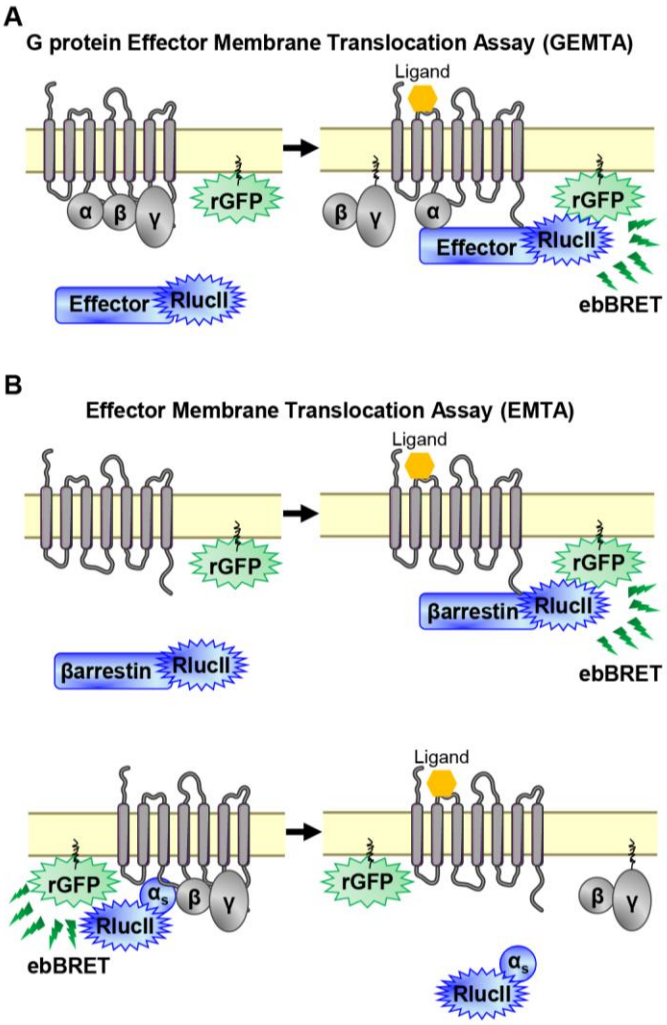

Figure 1. EMTA ebBRET platform to monitor G protein activation and βarrestin recruitment. (**A**) Schematic of the G protein Effector Membrane Translocation Assay (GEMTA) to monitor Gα protein activation. Upon receptor activation, RlucII-tagged effector proteins (Effector-RlucII) translocate towards and interact with active Gα subunits from each G protein family, leading to increased ebBRET. (**B**) Principle of the Effector Membrane Translocation Assay (EMTA) monitoring βarrestin recruitment to the plasma membrane (*top*) and $G\alpha_s$ activation (*bottom*). *Top*; upon receptor activation, RlucII-tagged βarrestins (βarrestin-RlucII) translocate to the plasma membrane, thus increasing ebBRET with rGFP-CAAX. *Bottom*; Internalization of activated RlucII-tagged $G\alpha_s$ ($G\alpha_s$-RlucII) following receptor stimulation decreases ebBRET with the membrane-anchored rGFP-CAAX.

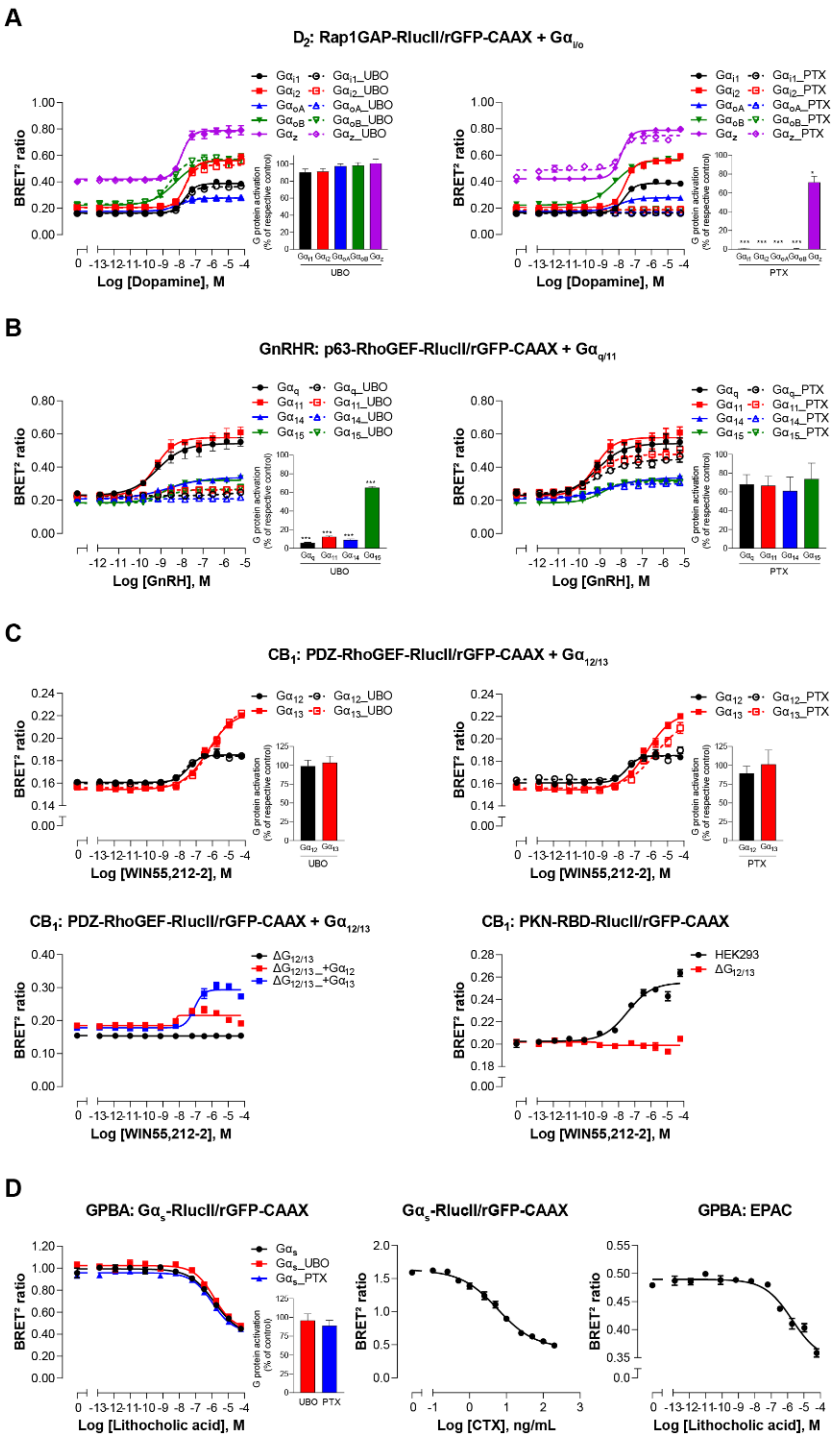

Figure 2. Validation of EMTA ebBRET-based platform to monitor Gα protein activation. (**A**) Pharmacological validation of the $G\alpha_{i/o}$ activation sensor. HEK293 cells were transfected with the D_2 receptor and the $G\alpha_{i/o}$ family-specific sensor, along with each $G\alpha_{i/o}$ subunit. Dose-response curve using the $G\alpha_{i/o}$ activation sensor, in the presence or absence of UBO-QIC (*left*) or PTX (*right*) inhibitors. *Insets*; E_{max} values determined from dose-response curves of inhibitor-pretreated cells. (**B**) Pharmacological validation of the $G\alpha_{q/11}$ activation sensor. HEK293 cells were transfected with the GnRH receptor and the $G\alpha_{q/11}$ family-specific sensors, along with each $G\alpha_{q/11}$ subunit. Dose-

response curve using $G\alpha_{q/11}$ activation sensor, in the presence or absence of UBO-QIC (*left*) or PTX (*right*) inhibitors. *Insets*; E_{max} values determined from dose-response curves of inhibitor-pretreated cells. (**C**) Validation of the $G\alpha_{12/13}$ activation sensor. Cells were transfected with the CB_1 receptor and one of the $G\alpha_{12/13}$ activation sensors, along with the $G\alpha_{12}$ or $G\alpha_{13}$ subunits. Dose-response curves of HEK293 cells (*top*) or the parental and devoid of $G_{12/13}$ ($\Delta G_{12/13}$) HEK293 cells (*bottom*) using the PDZ-RhoGEF-RlucII/rGFP-CAAX sensors (*top and bottom left*) or PKN-RBD-RlucII/rGFP-CAAX (*bottom right*), pretreated or not with UBO-QIC or PTX (*top*). Data are expressed as BRET ratio for the dose-response curves or expressed in % of respective control cells (E_{max} graphs) and are means ± SEM of 3 (**A**-**C**) or 4 (**D**) independent experiments. One Way ANOVA test (**A**) or Unpaired t test (**B**-**D**): *p < 0.05 and ***p < 0.001 compared to control cells. (**D**) Pharmacological validation of the $G\alpha_s$ activation sensor. HEK293 cells were transfected with the GPBA receptor and the $G\alpha_s$ activation (*left and central*) or the EPAC (*right*) sensors. *Left:* Dose-response curves using the $G\alpha_s$ activation sensor in the presence or absence of UBO-QIC or PTX, inhibitors of $G\alpha_q$ or $G\alpha_{i/o}$, respectively. *Central*: Dose-response activation of the $G\alpha_s$ sensor using CTX, a $G\alpha_s$ activator. *Right*: Dose-response curve using the EPAC sensor. *Inset*; E_{max} values determined from dose-response curves of inhibitors-pretreated cells.

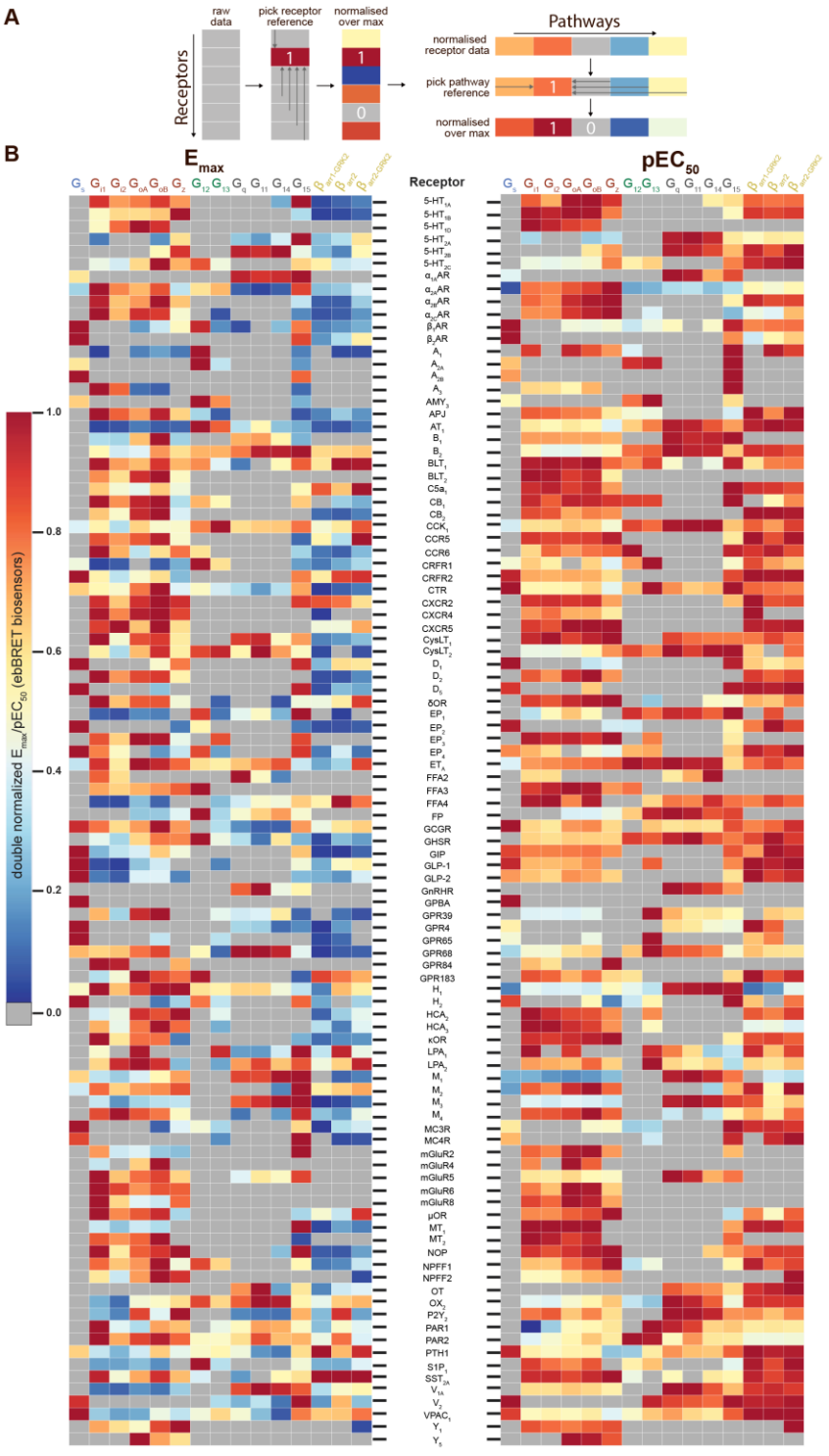

886

887 **Figure 3. Heatmaps illustrating the diversity of receptor-specific signaling signatures detected**
888 **with the EMTA ebBRET platform.** (**A**) First, values within each pathway were normalized relative
889 to the maximal response observed across all receptors (max. =1; *left*). These values were then
890 normalized across pathways for the same receptor, with the highest-ranking pathway serving as
891 the reference (=1; *right*). (**B**) Heatmap representation of double normalized E_{max} (*left*) and pEC_{50}
892 (*right*) data. Empty cells (grey) indicate no coupling.

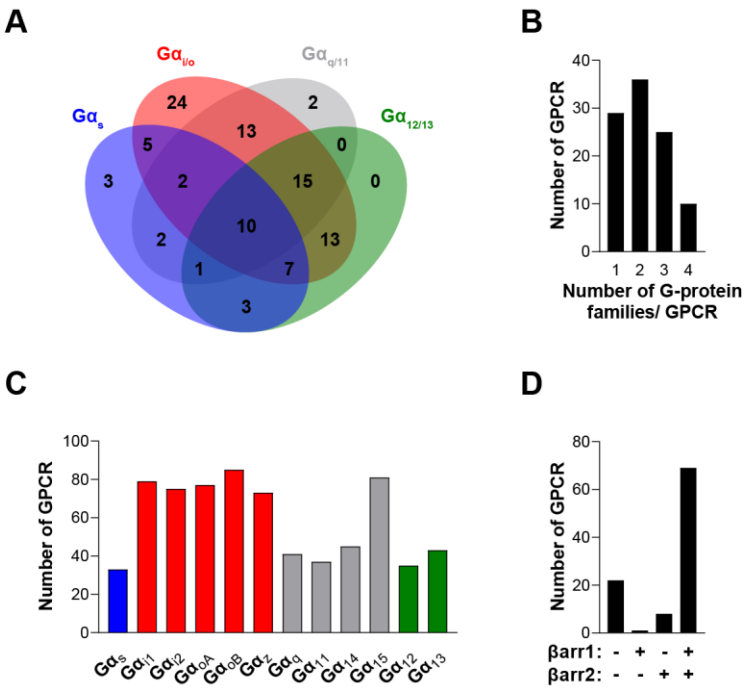

Figure 4. The EMTA ebBRET platform has a unique ability to uncover coupling selectivity between G protein families. (**A**) Venn diagram showing the numbers of receptors coupled to each G protein family in the EMTA ebBRET biosensor assay. (**B**) Evaluation of receptors coupling promiscuity: number of receptors that couple to members of 1, 2, 3 or 4 G protein families. (**C**) Determination of G protein subunit coupling frequency: number of receptors that activate each Gα subunit. (**D**) Proportion of receptors recruiting βarrestins: number of receptors that do not recruit (-/-) or that recruit either (+/- or -/+) or both (+/+) βarrestin isotypes. All data are based on double normalized E_{max} values from **Figure 3**.

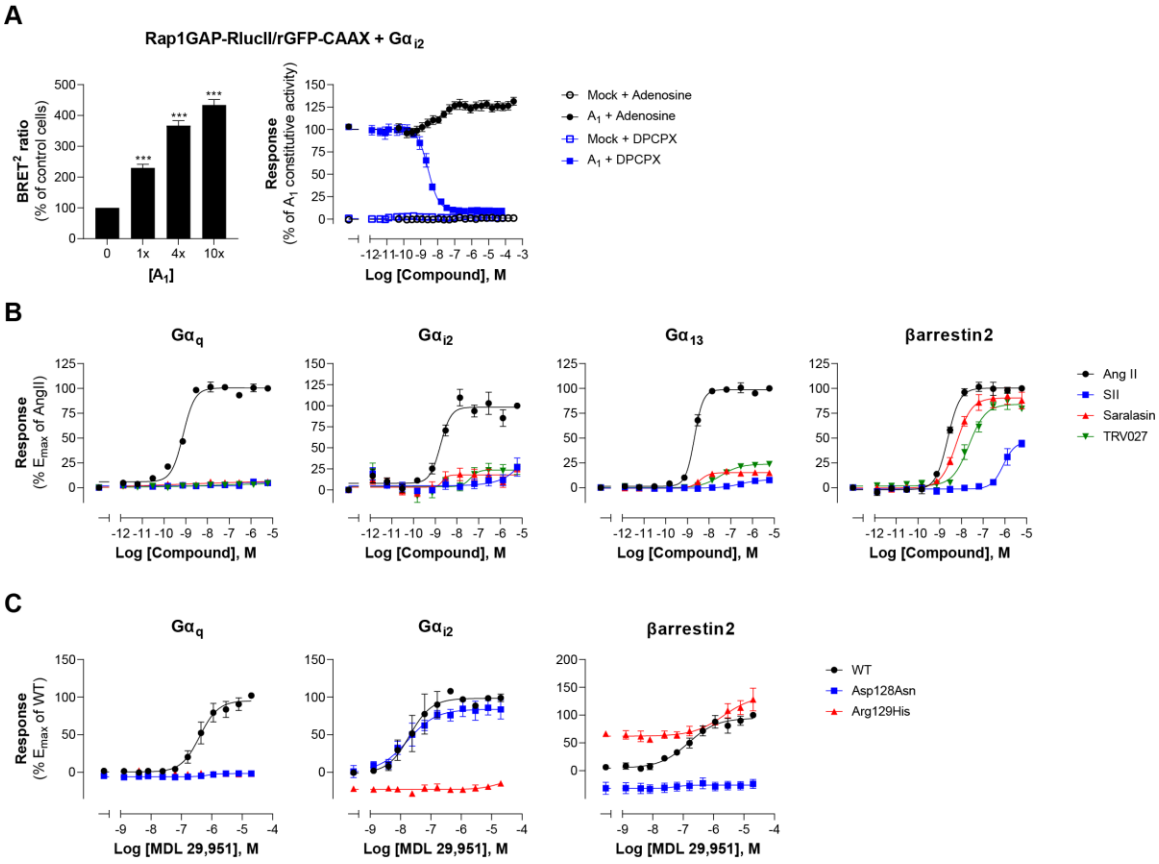

Figure 5. Multiple applications using the EMTA ebBRET platform. (**A**) Inverse agonist activity detection. *Left*: $G\alpha_{i2}$ activation in HEK293 cells transfected with the Rap1GAP-RlucII/rGFP-CAAX sensors with untagged $G\alpha_{i2}$ and increasing amount of A_1 receptor plasmid. Data are expressed in % of response obtained in control cells (0 ng of A_1) and are means ± SEM of 4-6 independent experiments. One Way ANOVA test: ***p < 0.001 compared to control cells. *Right:* HEK293 cells expressing the $G\alpha_{i2}$ activation sensor and control (Mock) or A_1 receptor plasmid were stimulated with increasing concentrations of the indicated compound. Data are expressed in % of constitutive response obtained in vehicle-treated A_1 transfected cells and are means ± SEM of 4-6 independent experiments. (**B**) Ligand-biased detection. Concentration-response curves of AT_1 for the endogenous ligand (Angiotensin II, AngII) and biased agonists [Sar1-Ile4-Ile8] AngII (SII), saralasin or TRV027. G-protein and βarrestin2 signaling activity were assessed by EMTA platform. Data are expressed in % of maximal response elicited by AngII and are means ± SEM of 3-6 independent experiments. (**C**) Functional selectivity of naturally occurring receptor variants. Concentration-response curves for WT or E/DRY motif Asp128Asn and Arg129His variants of GPR17 upon agonist stimulation in HEK293 cells co-expressing the indicated EMTA biosensor. Data are expressed in % of maximal response elicited by WT receptor and are means ± SEM of 3 independent experiments.

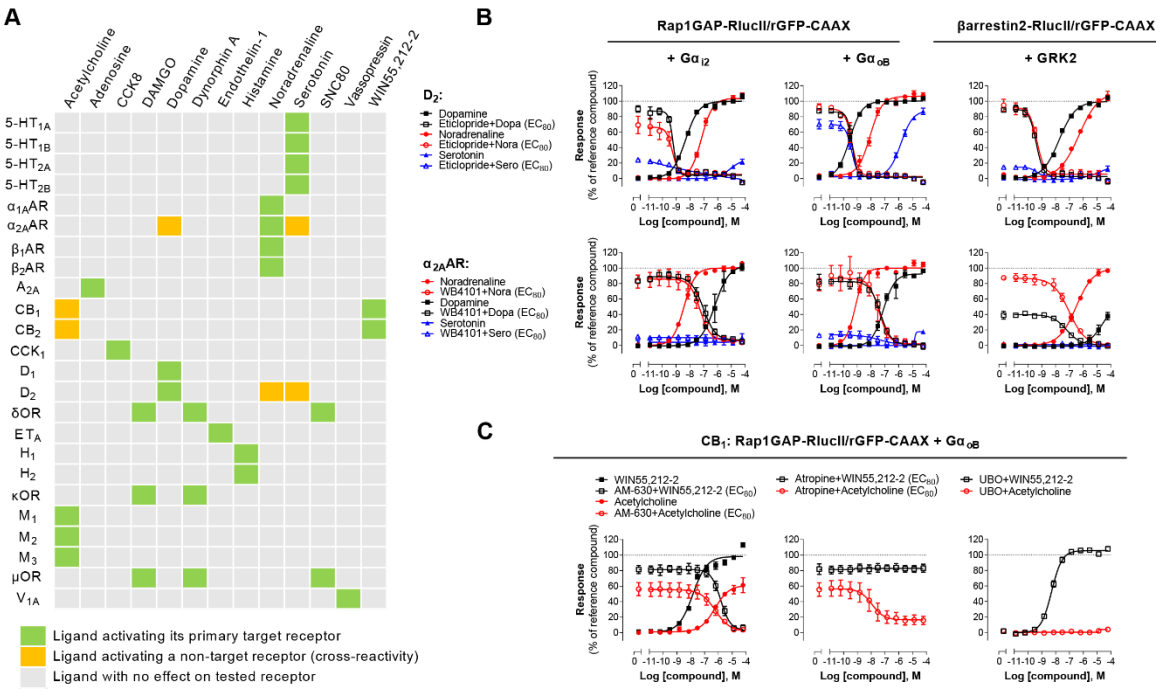

Figure 6. Detection of direct (*cis*) and indirect (*trans*) mechanisms of ligand polypharmacology using the G_z/G_{15} biosensor. (**A**) Test of the G_z/G_{15} biosensor on a safety target panel. ebBRET signal was measured before and after stimulation with the indicated ligand in HEK293 cells transfected with the combined G_z/G_{15} biosensor and one of the 24 receptors listed. (**B**) Direct (*cis*) activation of D_2 and α_{2A}AR by others natural ligands. For the agonist mode read, HEK293 cells expressing D_2 or α_{2A}AR and either the $G\alpha_{i2}$, $G\alpha_{oB}$, or the βarrestin2+GRK2 sensors were stimulated with increasing concentrations of the indicated ligand. For the antagonist mode read, cells were pretreated with increasing concentrations of the selective D_2 antagonist eticlopride or the selective α_{2A}AR antagonist WB4101 before stimulation with an EC_{80} of the indicated ligand. Data are means ± SEM from 3-4 independent experiments and expressed in % of the response elicited by dopamine or noradrenaline for D_2 and α_{2A}AR expressing cells, respectively. (**C**) Indirect (*trans*) activation of CB_1 by acetylcholine. For the agonist mode read, HEK293 cells expressing CB_1 and the Rap1GAP-RlucII/rGFP-CAAX sensors with untagged $G\alpha_{oB}$ were stimulated with increasing concentrations of the indicated ligand. For the antagonist mode read, same cells were pretreated or not with increasing concentrations of the CB inverse agonist AM-630 (*left*) or the cholinergic antagonist atropine (*central*) before stimulation with an EC_{80} of the indicated ligand. To evaluate the contribution of $G_{q/11}$-coupled receptor, cells were pretreated with the $G\alpha_q$ inhibitor UBO-QIC and then stimulated with increasing concentrations of the indicated ligand (*right*). Data are means ± SEM from 3-5 independent experiments and expressed in % of the response elicited by WIN55,212-2.

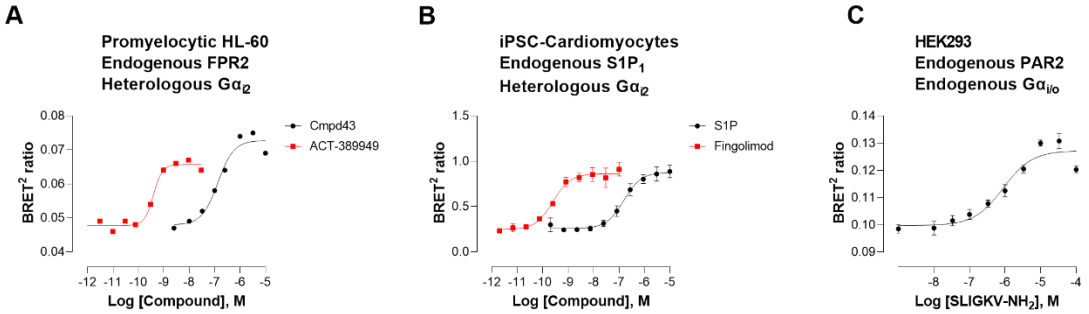

940

941 **Figure 7. Detection of endogenous receptor- and/or G protein-mediated responses in cells with**
942 **the EMTA ebBRET platform.** (**A**) Dose-dependent activation of $G\alpha_{i2}$ protein by endogenous FPR2
943 in promyelocytic HL-60 cells transfected with $G\alpha_{i2}$ activation sensors (Rap1GAP-RlucII/rGFP-CAAX
944 + $G\alpha_{i2}$). (**B**) Dose-dependent activation of $G\alpha_{i2}$ protein by endogenous $S1P_1$ receptor in iPSC-
945 derived cardiomyocytes cells transfected with $G\alpha_{i2}$ activation sensors (Rap1GAP-RlucII/rGFP-
946 CAAX + $G\alpha_{i2}$). (**C**) Dose-dependent activation of endogenous $G\alpha_{i/o}$ proteins by endogenous PAR2
947 receptor in HEK293 cells transfected with $G\alpha_{i/o}$ activation sensor (Rap1GAP-RlucII/rGFP-CAAX).
948 Data are the mean ± SEM of 3 independent experiments and are expressed as $BRET^2$ ratio.